Journal of Applied Physics

RESEARCH ARTICLE | MAY 19 2008

Reaction mechanisms during plasma-assisted atomic layer deposition of metal oxides: A case study for Al_2O_3

S. B. S. Heil; J. L. van Hemmen; M. C. M. van de Sanden; W. M. M. Kessels

J. Appl. Phys. 103, 103302 (2008)
https://doi.org/10.1063/1.2924406

Reaction mechanisms during plasma-assisted atomic layer deposition of metal oxides: A case study for Al_2O_3

S. B. S. Heil,[a] J. L. van Hemmen, M. C. M. van de Sanden, and W. M. M. Kessels[b]
Department of Applied Physics, Eindhoven University of Technology, P.O. Box 513, 5600 MB Eindhoven, The Netherlands

(Received 14 November 2007; accepted 17 March 2008; published online 19 May 2008)

Plasma-assisted atomic layer deposition (ALD) of metal oxide films is increasingly gaining interest, however, the underlying reaction mechanisms have rarely been addressed. In this work, a case study is presented for the plasma-assisted ALD process of Al_2O_3 based on $Al(CH_3)_3$ dosing and O_2 plasma exposure. A complementary set of time-resolved *in situ* diagnostics was employed, including spectroscopic ellipsometry, quartz crystal microbalance, mass spectrometry, and optical emission spectroscopy. The saturation of the $Al(CH_3)_3$ adsorption reactions was investigated, as well as the reaction products created during both the precursor dosing and the plasma exposure step. The generality of the observations was cross-checked on a second commercial ALD reactor. The main observations are as follows: (i) during the precursor dosing, the $Al(CH_3)_3$ predominantly binds bifunctionally to the surface at 70 °C through a reaction in which H is abstracted from the surface and CH_4 is released into the gas phase; (ii) during the plasma exposure, O radicals in the plasma are consumed at the surface by combustionlike reactions with the surface $-CH_3$ ligands, producing mainly H_2O, CO_2, and CO; (iii) small gas phase densities of CH_4 and higher hydrocarbons (C_2H_x) are also present during the O_2 plasma exposure step indicating complementary surface reactions including a secondary thermal ALD-like reaction by the H_2O produced at the surface; (iv) the plasma and its optical emission are strongly affected by the surface reaction products released in the plasma. In the latter respect, optical emission spectroscopy proved to be a valuable tool to study the surface reaction products during the plasma exposure as well as the saturation of the surface reactions. The implications of the experimental observations are addressed and it is discussed that the reaction mechanisms are generic for plasma-assisted ALD processes based on metal organic precursors and O_2 plasma as oxidant source. © *2008 American Institute of Physics*.
[DOI: 10.1063/1.2924406]

I. INTRODUCTION

The synthesis of very thin metal oxide films by atomic layer deposition (ALD) is currently a very active research field. Investigations into various metal oxide materials for applications in semiconductor devices such as gate oxide in complementary-metal-oxide-semiconductor gate stacks and as dielectric layer in dynamic-random-access-memory devices had led to a rapid increase in the number of ALD processes developed. In many of the metal oxide ALD processes metal organic precursors are employed and H_2O is used as oxidant.[1] However, since recently, ALD processes in which O_3 or an O_2 plasma is used as an alternative oxidant source are gaining increasingly more attention. In these latter processes the oxidant is more reactive than H_2O and, therefore, the surface reactions rely less on thermal activation by the substrate temperature. For example, when an O_2 plasma is used, chemical activation of the oxidant has already occurred in the gas phase and, therefore, the use of a lower deposition temperature is in many cases facilitated. Furthermore, for some materials it has been reported that improved film properties are obtained when using O_3 or O_2 plasma instead of H_2O.[2–8] The potentially more favorable process settings (e.g., in terms of substrate temperature and purge times) as well as the potentially improved material properties obtained for the O_3 and O_2 plasma based ALD processes have also contributed to an increased interest into ALD by other fields of technology than semiconductor industry. Potential application of ALD films in areas such as microsystems, solar cells, flexible electronics, energy storage, and photonics have recently been reported.[9–19]

While the material properties and functionality of the films have already been investigated in relative detail, the reaction mechanisms leading to film growth in the O_3 and O_2 plasma based ALD processes have hardly been addressed. Very recently, however, theoretical and experimental investigations of the reaction mechanism of Al_2O_3 ALD from $Al(CH_3)_3$ [trimethylaluminum (TMA)] precursor and O_3 were reported by Elliott *et al.*[20] and Goldstein and George.[21] Our research group recently published a first study about the reaction mechanism of plasma-assisted ALD of Al_2O_3 using $Al(CH_3)_3$ and O_2 plasma.[22] The current article is a follow up on this earlier work and a more extended study of the plasma-assisted ALD process of Al_2O_3 will be presented.

Due to its excellent dielectric properties, its good adhesion to many surfaces, and its high thermal and chemical stability, Al_2O_3 is a very relevant material for a wide range

[a]Electronic mail: s.b.s.heil@tue.nl.
[b]Author to whom correspondence should be addressed. Electronic mail: w.m.m.kessels@tue.nl.

of applications. Furthermore, the thermal ALD process of Al_2O_3 using $Al(CH_3)_3$ and H_2O is considered to be a model system for ALD film growth of metal oxides.[1] The ALD reaction mechanisms during the $Al(CH_3)_3$ and the H_2O step have been thoroughly investigated both experimentally and theoretically.[23–31] From these investigations, it has been established that Al_2O_3 growth by thermal ALD occurs via the following successive "half-reactions:"[32]

$$AlOH_{(s)} + Al(CH_3)_{3(g)} \rightarrow AlOAl(CH_3)_{2(s)} + CH_{4(g)}, \quad (1)$$

$$Al - CH_{3(s)} + H_2O_{(g)} \rightarrow AlOH_{(s)} + CH_{4(g)}, \quad (2)$$

where (s) and (g) represent surface groups and gas species, respectively. The chemisorption of $Al(CH_3)_3$ and H_2O on the surface is a Lewis acid-base reaction in which methyl ligands (CH_3^-) and hydroxyl protons (H^+) combine in a Brønsted acid-base reaction and are eliminated as CH_4.[20,28,29,33] For Al_2O_3 as well as for some other metal oxides, the amount of material deposited per cycle was found to directly relate with the substrate temperature dependent $-OH$ density on the surface.[34,35]

For the plasma-assisted ALD process of Al_2O_3 based on $Al(CH_3)_3$ dosing and O_2 plasma exposure, we recently presented compelling evidence that the $Al(CH_3)_3$ chemisorption step appears very similar as in the thermal ALD process with H_2O.[22] Nonetheless, the oxidation step by the O_2 plasma appeared to be very different from the H_2O based process. It was demonstrated that combustionlike reactions by the plasma generated O radicals removed the $-CH_3$ ligands from the surface because combustion products such as CO_2 and H_2O were detected by mass spectrometry.[22] Furthermore, a small signal due to the presence of CH_4 during the plasma exposure step indicated that the formed H_2O byproduct induces a secondary thermal ALD-like reaction pathway. Previously such secondary reaction pathway, in which the reaction products of the oxidation step play a role in the surface chemistry, was speculated upon.[2,36] In this article we present corroborating evidence and additional details that support the previously proposed reaction mechanism. A more extensive and complementary data set is reported as obtained by a combination of several *in situ* diagnostics such as spectroscopic ellipsometry (SE), quartz crystal microbalance (QCM) measurements, quadrupole mass spectrometry (QMS), and optical emission spectroscopy (OES). More specifically, extensive data on the saturation of the $Al(CH_3)_3$ chemisorption reaction are presented. The previous observations are also corroborated by an additional data set obtained on a commercial 200 mm ALD reactor (Oxford Instruments FlexAL). More insight into several aspects of the reaction mechanism of plasma-assisted ALD of Al_2O_3 has been obtained: QMS signals for mass-to-charge ratios of $m/z = 24-30$ suggest the presence of small amounts of C_2H_x during the plasma exposure, in addition to the earlier detected presence of H_2O, CO_2, CO, and CH_4.[22] By OES with an extended wavelength range in the UV, the presence of OH* emission was also identified during the plasma step. Furthermore, it has been demonstrated that the saturation conditions for Al_2O_3 film growth can be determined not only directly via the use of film growth monitoring techniques, such as spectroscopic ellipsometry and quartz crystal microbalance, but also indirectly by gas phase diagnostics, such as OES and QMS. On the basis of the results reported a more complete picture of the reaction mechanisms during plasma-assisted ALD of Al_2O_3 will be presented. Finally, from this case study of Al_2O_3, the implications for plasma-assisted ALD of other metal oxide films grown from metal organic precursors and O_2 plasma will be briefly discussed.

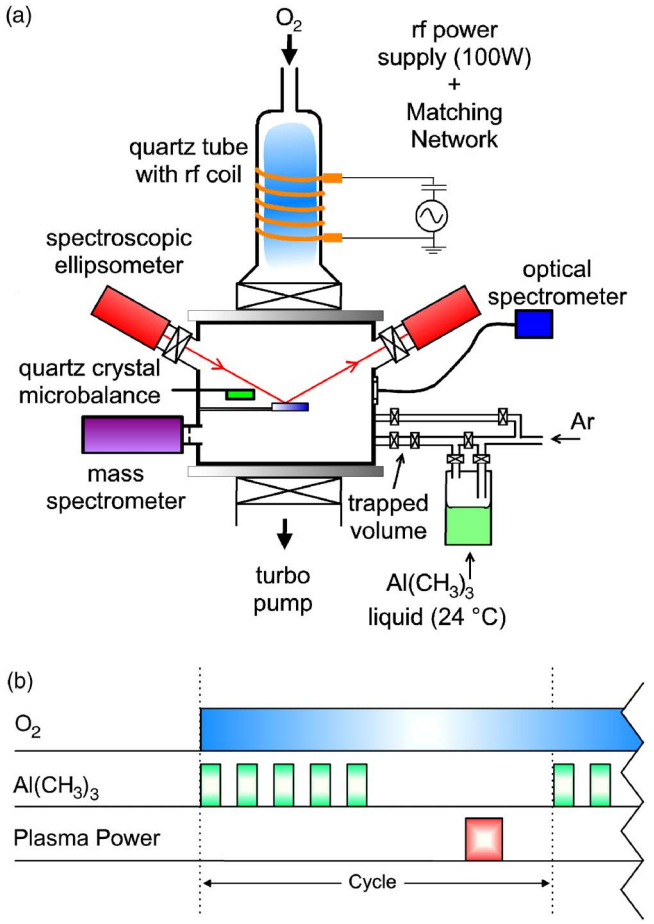

FIG. 1. (Color online) (a) Schematic of the homebuilt remote plasma ALD reactor "ALD-I" with the *in situ* diagnostics indicated. (b) Schematic layout of the plasma-assisted ALD cycle for Al_2O_3 deposition. The precursor dosing by several successive, small $Al(CH_3)_3$ exposures per cycle is indicated.

II. EXPERIMENTAL

A. ALD-I reactor

1. Reactor setup

Most of the experiments were carried out on a homebuilt remote plasma ALD reactor referred to as "ALD-I," which is schematically represented in Fig. 1(a). The reactor has been described in detail in our previous work with respect to the deposition of TiN and TaN films using a N_2-H_2 plasma.[37,38] Briefly, it consists of a remotely placed inductively coupled plasma source which is powered at a radiofrequency of 13.56 MHz and at a power of 100 W. For Al_2O_3 deposition the source is operated on O_2 gas (purity >99.999%). The plasma source is connected to a wall heated deposition chamber where substrates can be placed on a individually heated stainless steel substrate holder. $Al(CH_3)_3$ (Akzo No-

bel, semiconductor grade, purity >99.9999%) contained in a stainless steel bubbler and kept at room temperature was mounted to the precursor delivery line in which a small trapped volume (~0.25 cm^3) was present in between two pneumatic valves. It should be noted that $Al(CH_3)_3$ forms a dimeric molecule in the liquid phase and in the gas phase at low temperatures through a bridged structure via the methyl groups.[39,40] At temperatures ≥70 °C and at low pressures the $Al(CH_3)_3$ is predominantly in the monomer phase.[41]

2. Pulsing of the reactants

A schematic of the ALD cycle used in these experiments is shown in Fig. 1(b). A continuous flow of O_2 through the plasma source served both as plasma gas and as a purge gas. Since $Al(CH_3)_3$ and O_2 do not react in the gas phase[22,42,43] it can be introduced into the O_2 background. The amount of precursor dosed per cycle was set by the number of successive, small $Al(CH_3)_3$ exposures introduced into the reactor through alternatively evacuating (1 s) and refilling (1 s) the small trapped volume in the precursor delivery line. After a purging period, an O_2 plasma exposure was applied for a number of seconds by turning on the rf power. In the current investigation the implemented purge times were set such to allow for a complementary study by all diagnostics. During the cycle the pressure in the reactor was approximately constant at 7.5 mTorr. The deposition temperature was set to 70 °C by wall heating of the reactor.

3. In situ diagnostics

For *in situ* film measurements, a rotating compensator SE (J.A. Woollam, Inc. M2000U) with a wavelength range of 245–1000 nm was mounted on the reactor. The angle of incidence on the substrates was 68° with the substrate normal. SE data were typically measured after every ten completed Al_2O_3 ALD cycles. Crystalline silicon (*c*-Si) was used as substrate material, which was either plasma oxidized for 5 min prior to deposition or contained a 400 nm thick thermal SiO_2 layer on top. The thickness of the Al_2O_3 was determined by fitting the SE data with a Cauchy model using the Woollam WVASE software. The value of the refractive index at a photon energy of 2 eV ranged typically between 1.60 and 1.65 for the Al_2O_3 films investigated by SE.

Film growth was also monitored by a QCM. Gold covered AT-cut quartz crystals with an oscillation frequency of 6 MHz were mounted in a Maxtek 150BSH bakeable crystal holder positioned in close proximity to the substrate holder and with the crystal surface facing down (i.e., not facing the plasma source). The crystals were first coated with a "fresh" plasma-assisted ALD Al_2O_3 film before taking any film growth data. The QCM signal was monitored using a Maxtek TM400 thickness monitor which was interfaced with a computer at a data acquisition rate of 10 Hz. The extremely high sensitivity of the QCM to surface temperature fluctuations on the crystal progresses with temperature and, consequently, a careful interpretation of the measured signal is required.[44,45] This high sensitivity of the QCM is the reason for controlling the temperature at 70 °C by uniform wall heating in this particular experiment, as described above. In addition, pressure variations in the reactor were adequately minimized by continuously flowing the O_2 gas. The QCM results are expressed in terms of mass gain with the unit hertz.[46]

The gas composition was measured by a differentially pumped QMS (Pfeifer QME 200, mass-to-charge ratio m/z =0–100) fitted at the side of the reactor. The gas sampling took place through a 150 μm diameter pinhole keeping the pressure in the mass spectrometer within the working range ($<10^{-5}$ Torr) for the secondary electron multiplier to operate. The electron impact ionization by ~70 eV electrons in the mass spectrometer leads to fragmentation or "cracking" of incoming gas species. The identification of the parent molecules was therefore performed on the basis of its so-called cracking pattern. The cracking pattern of some molecules (CO, CO_2, and $Al(CH_3)_3$) was measured specifically for our QMS by introducing calibration gases yielding good agreement with data reported in the literature. To achieve sufficient time resolution, time-resolved measurements were carried out by monitoring only two mass-to-charge ratios (m/z) at a time with an integration time of 10 ms. One of the two masses selected served as a reference signal, while the other mass (in the range of m/z=10–75) was varied over several runs. In the current measurements m/z=32 (O_2^+) was taken as reference as there is a continuous flow of O_2 into the reactor. Data are typically taken over ten ALD cycles, and on the basis of the m/z=32 (O_2^+) signal the measurements were synchronized afterwards. This procedure allowed for constructing a time-resolved mass scan of several masses with an adequate time resolution.

OES measurements were carried out by measuring the plasma emission just above the substrate holder using an Ocean Optics USB2000 spectrometer having a wavelength detection range of 250–870 nm and a spectral resolution of approximately 1 nm. The emission by the plasma was coupled into the spectrometer by placing an optical fiber with a small aperture (~100 μm diameter) close to one of the quartz windows on the main chamber. Time dependent measurements were carried out by repetitively acquiring full spectra (250–870 nm) with an integration time of 100 ms. The option in the software for selecting emission peaks in the spectrum and measuring the signal height as a function of time was also used to monitor excited plasma species during the plasma exposure step.

B. FlexAL reactor

A similar, but less extensive *in situ* study of the Al_2O_3 process was carried out in the commercial 200 mm FlexAL reactor from Oxford Instruments. Both the FlexAL reactor itself and the characteristics of the deposition process of Al_2O_3 by remote plasma ALD using this reactor have been described in our previous work.[3,47] One main difference with the experiments carried out on the homebuilt ALD-I reactor described above is the method of precursor dosing. In the FlexAL a single dose is injected into the deposition chamber using a fast open-close (20 ms) Swagelok ALD valve positioned in the precursor delivery line. In all experiments an open-close time of 20 ms was used for $Al(CH_3)_3$ dosing leading to saturated ALD reactions for Al_2O_3. Furthermore, a

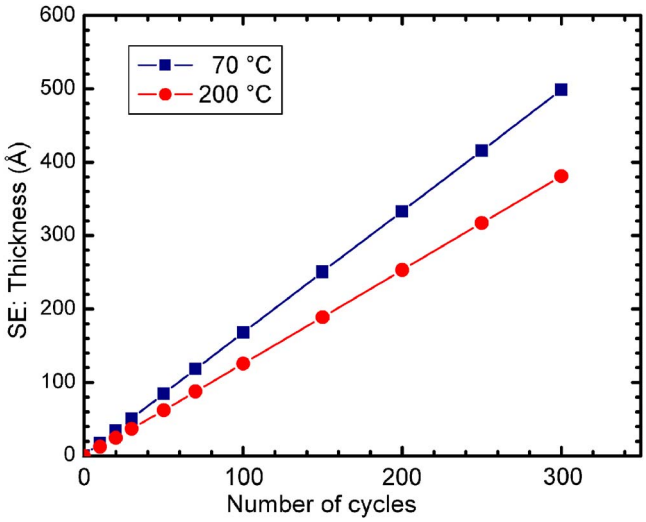

FIG. 2. (Color online) Thickness of Al_2O_3 as a function of the number of cycles as measured by SE for deposition temperatures of 70 and 200 °C. The data shown are for films deposited on plasma oxidized *c*-Si substrates.

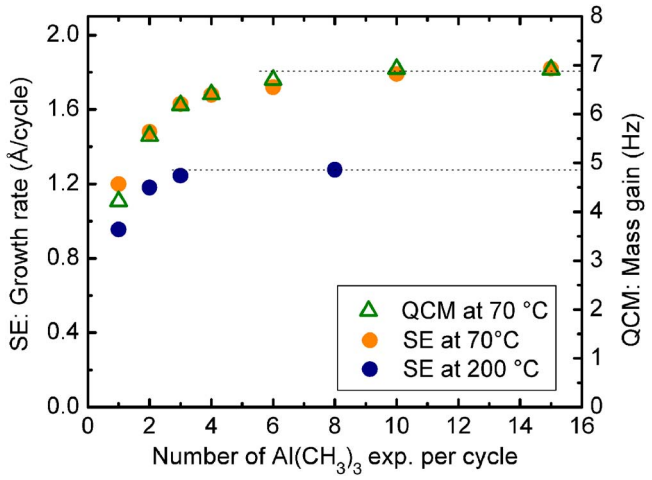

FIG. 3. (Color online) Growth rate per cycle as measured by SE at deposition temperatures of 70 and 200 °C as a function of the number of successive $Al(CH_3)_3$ exposures used per ALD cycle. Also the mass gain determined by QCM measurements at 70 °C is given.

continuous O_2 flow of 60 SCCM (SCCM denotes cubic centimeter per minute at STP) was applied through the plasma source and the pressure in the reactor was kept constant at 15 mTorr. The intermitting purge time between precursor and plasma was 3 s, the plasma exposure was set to 4 s, and the purge between plasma and precursor was 0.5 s. Both the reactor walls and the substrate holder were not heated and remained at a temperature of approximately 25 °C.

Similar to the ALD-I setup, the FlexAL was equipped with a spectroscopic ellipsometer, a mass spectrometer, and optical emission spectroscopy. The SE configuration was similar to the ALD-I.[3] The mass spectrometer (QMS, Pfeifer QME 200, m/z=0–200) was differentially pumped and the only difference with the ALD-I setup is that this mass spectrometer has an extended mass-to-charge (m/z) range and consequently a higher signal-to-noise ratio, especially for m/z ratios >40. Optical emission spectroscopy was performed using the same equipment as for the ALD-I. The plasma emission was collected through a quartz window at the top of the plasma source probing the emission from both the plasma source region and the downstream reactor region by line-of-sight measurement. This configuration was chosen because probing the emission downstream from the side of the reactor lead to a poor signal-to-noise-ratio at the high time resolution (≤100 ms) desired. The data analysis of the *in situ* diagnostics on the FlexAL reactor was identical to the data analysis on the ALD-I reactor.

III. RESULTS

A. *In situ* thickness monitoring by SE

In our previous work, it was established that *in situ* spectroscopic ellipsometry is a valuable tool to monitor ALD film growth.[3,38,48] In the current work the plasma-assisted ALD process of Al_2O_3 was characterized at substrate temperatures of 70 and 200 °C. Figure 2 shows the results obtained for a plasma exposure time of 2 s. The substrates were plasma oxidized Si samples prepared *in situ*. A clear linear increase in thickness with the number of cycles can be observed at both deposition temperatures. A thickness increase per cycle of 1.66 ± 0.02 Å at 70 °C and 1.27 ± 0.02 Å at 200 °C was calculated from the slope of the data shown in Fig. 2. No significant initial growth delay was observed in the first few cycles of Al_2O_3 deposition both on the plasma oxidized Si samples and on the thermal oxide covered *c*-Si.

In situ SE was used to determine the saturated precursor dosing regime associated with ALD film growth. The amount of $Al(CH_3)_3$ introduced per precursor exposure was varied using the trapped volume in the precursor line as described earlier. The amount of precursor is fixed by the size of the trapped volume (~0.25 cm^3) and the total precursor dose can therefore be varied by varying the number of successive precursor exposures used per cycle. The thickness increase per cycle (i.e., growth rate, sometimes also referred to as growth per cycle) is shown in Fig. 3 as a function of the number of successive $Al(CH_3)_3$ exposures per cycle at 70 and 200 °C. The figure reveals that saturated growth is obtained for a total precursor dose consisting of more than six $Al(CH_3)_3$ exposures per cycle for both temperatures.

Under saturated $Al(CH_3)_3$ dosing conditions (i.e., more than six exposures) and 4 s plasma exposure the growth rate is 1.80 ± 0.02 Å/cycle at 70 °C and 1.27 ± 0.02 Å/cycle at 200 °C. These values are higher than typically reported for thermal ALD process using H_2O, i.e., 1.1 Å/cycle at 70 °C and 1.0 Å/cycle at 200 °C.[24,25] Also for the thermal ALD process with O_3 lower growth rates were observed (1.1 Å/cycle at 70 °C and 0.8 Å/cycle at 200 °C).[5,49] A higher growth rate has been reported earlier for both remote and direct plasmas compared to thermal ALD for identical deposition temperature settings.[3,50,51] We would like to note that the H_2O based process suffers from the so-called "soft saturation" behavior, especially at low temperatures. High doses of H_2O have been found necessary to reach saturated film growth.[3,25,52] Not fully saturated growth might therefore be a reason for the lower growth rate reported for the thermal process based on H_2O at 70 °C. A related aspect is that also very long purge times are required for removal of H_2O from

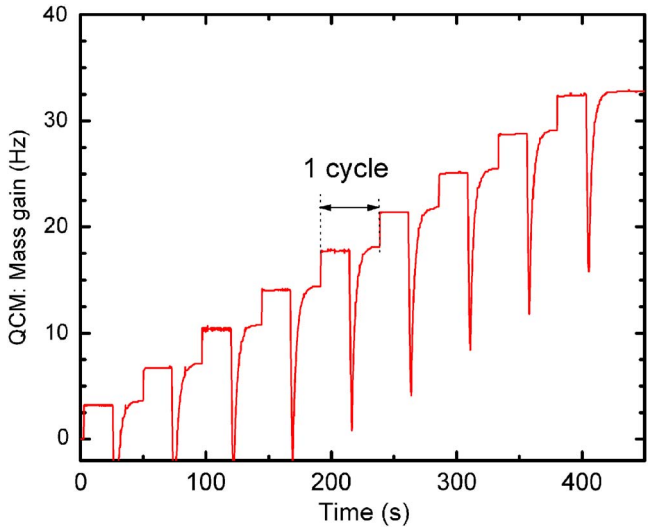

FIG. 4. (Color online) QCM measurements during plasma-assisted ALD of Al_2O_3 at a deposition temperature of 70 °C. The mass gain is shown for ten reaction cycles with the length of one ALD cycle being indicated. The precursor dose is smaller than necessary for saturation of the surface reactions.

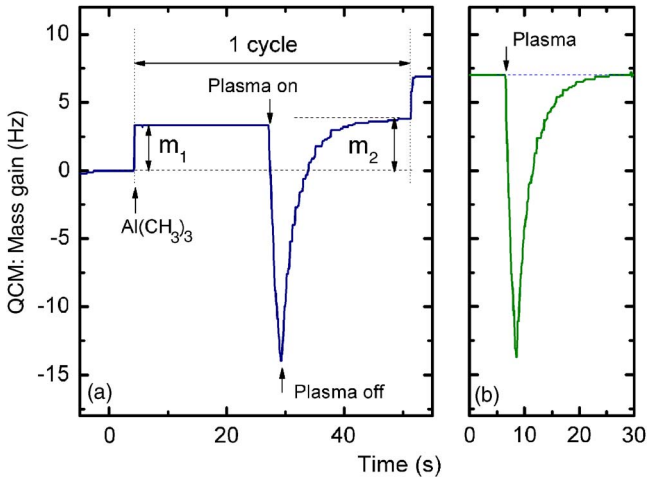

FIG. 5. (Color online) Detailed view of the QCM measurement at 70 °C of (a) a complete ALD cycle with $Al(CH_3)_3$ dosing and O_2 plasma exposure and (b) O_2 plasma exposure without preceding $Al(CH_3)_3$ dosing. The introduction of $Al(CH_3)_3$ and the start and end of the O_2 plasma exposure are indicated.

the reactor. These long purge times provide more time for dehydroxilation reactions,[1,29] lowering the surface –OH density. One of the benefits of ALD using O_3 or O_2 plasma as oxidant sources is that the purge times do not have to be severely extended to maintain proper ALD film growth at low deposition temperatures (<100 °C).[3,5]

B. Mass uptake measurements by QCM

Quartz crystal microbalance measurements were used to monitor the mass uptake during a cycle at a substrate temperature of 70 °C. Figure 4 shows the mass gain recorded by QCM for ten ALD cycles using only one single $Al(CH_3)_3$ exposure (i.e., a nonsaturated dose) per cycle and a plasma exposure time of 2 s. The QCM reveals a stepwise increase in mass in each ALD cycle. Also a negative spike is observed during every O_2 plasma step but this behavior can be attributed to a plasma artifact as will be discussed below. The mass gain was also measured in an experiment in which the total precursor dose was varied in a similar experiment as for the SE measurements. These results, obtained at 70 °C, are also included in Fig. 3. From Fig. 3, it is evident that also the QCM measurements reveal saturated growth for a dose consisting of more than six precursor exposures per cycle, in perfect agreement with the SE measurements.

A detailed view of the QCM signal for one ALD cycle is presented in Fig. 5. The time at which precursor valve was opened and the period during which the plasma exposure was active are indicated. When $Al(CH_3)_3$ is introduced into the reactor the chemisorption of the precursor to the surface can be observed in the form of a large stepwise increase in mass (m_1) [Fig. 5(a)]. At the moment when the plasma is switched on, a sharp downward spike in the signal can be observed. Different from thermal ALD, the occurrence of electrical charging by the presence of ions and electrons or possibly plasma induced heat transfer apparently interferes with a proper measurement during the plasma exposure. The spike is a true plasma artifact, corroborated by the fact that a similar spike is also observed when only the plasma is pulsed [i.e., no $Al(CH_3)_3$ dose has preceded the plasma exposure], as is presented in Fig. 5(b). In both cases the signal slowly recovers to its genuine level after the plasma is switched off (~20 s). The main difference, however, is that in Fig. 5(a) a small increase in mass (m_2-m_1) can be observed after the plasma exposure. This increase in mass is not observed when the precursor has not been introduced [see Fig. 5(b)]. The mass increase can be related to the oxidation of bonded precursor and the replacement of the surface functional groups.

The behavior in Fig. 5(a) shows resemblance to what has previously been observed during QCM studies of thermal ALD of Al_2O_3 at 70 °C. In these experiments during both the $Al(CH_3)_3$ and the H_2O dosing, an increase in mass was observed.[25] Although for plasma-assisted ALD of Al_2O_3 the exact reaction mechanism has still not been clearly established, when following the procedure introduced by Rahtu and Ritala,[53] the origins for the mass gain after the $Al(CH_3)_3$ dose (m_1) and the plasma exposure (m_2) can be defined as

$$m_1 = M[\mathrm{Al(CH_3)_3}] - n \cdot M(\mathrm{CH_4}), \tag{3}$$

$$m_2 = M(\mathrm{AlO_{3/2}}), \tag{4}$$

where $M[Al(CH_3)_3]$, $M(AlO_{3/2})$, and $M(CH_4)$ represent the masses of the species involved, 72, 51, and 16 amu, respectively. On the basis of the previous measurements we can assume that reaction (3) occurs during the $Al(CH_3)_3$ dosing in which n $-CH_3$ ligands leave to the gas phase as CH_4 molecules.[22] Furthermore, for simplicity after the plasma step a complete Al_2O_3 layer is considered to have been formed. The possible presence of H on the surface after the plasma step is discarded since its mass is small compared to the other masses involved. On the basis of these assumptions the number of $-CH_3$ ligands released from the surface into the gas phase can be calculated by rewriting the ratio of the mass uptake after the two half-reactions (m_1/m_2) to

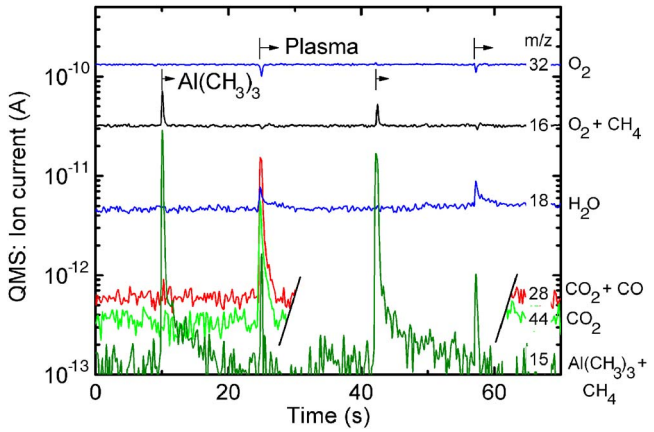

FIG. 6. (Color online) Time-resolved QMS for two plasma-assisted ALD cycles of Al_2O_3. The most likely parent molecules contributing to the signals at the selected mass-to-charge ratios (m/z) are indicated. For clarity purposes, the $m/z=28$ and $m/z=44$ signals are omitted during the second cycle.

$$n = \frac{M[\mathrm{Al(CH_3)_3}] - (m_1/m_2)\cdot M(\mathrm{AlO_{3/2}})}{M(\mathrm{CH_4})}, \tag{5}$$

For a saturated dose at 70 °C it was calculated using Eq. (5) that, on average, $n \sim 1.8$ ($-CH_3$) ligands per chemisorbed $Al(CH_3)_3$ molecule are released from the surface as CH_4. This indicates that $Al(CH_3)_3$ predominantly binds bifunctionally to the surface, i.e., on two surface groups, expectedly creating predominantly $(-O-)_2Al(CH_3)$ surface groups. For thermal ALD with H_2O as oxidant source, values between $n=1$ and $n=2$ have been reported by QMS and QCM for the 150–350 °C range. The values are somewhat closer to $n=2$ at the lower temperature side, whereas QCM yielded also somewhat higher values than QMS over the full temperature range.[24]

C. Investigation of reaction products by QMS

The gas species injected in the reactor as well as the stable gas species created by the surface reactions were measured using QMS. To achieve sufficient time resolution, the measurement procedure as outlined in the experimental section (Sec. II B) was employed. The QMS signals of the m/z ratios which showed the largest response to the ALD process are shown in Fig. 6 for two ALD cycles. The most likely parent molecules leading to the signals shown have been indicated in the figure. As mentioned earlier, the signals can either be due to direct ionization or dissociative ionization (cracking) of the corresponding molecule. Since a continuous O_2 flow was used a relatively high signal was measured at $m/z=32$ (O_2^+) and $m/z=16$ (O^+) due to the (dissociative) ionization of O_2 in the mass spectrometer. Furthermore, a relatively high signal at $m/z=18$ was measured (ion current of 4.5×10^{-12} A) which can be attributed to H_2O. It is generally difficult to remove H_2O from the vacuum system, including both the ALD reactor and the differentially pumped QMS housing. The other masses which are shown in Fig. 6 are $m/z=15$ (CH_3^+), 28 (CO^+), and 44 (CO_2^+). These signals have their baseline close to the noise level of the mass spectrometer (ion current of 10^{-13} A). For clarity purposes, the $m/z=28$ and $m/z=44$ signals are omitted during the second cycle in Fig. 6.

During $Al(CH_3)_3$ dosing peaks can be observed at $m/z=15$ (CH_3^+) and, albeit less clear due to the O_2 background, also at $m/z=16$ (CH_4^+). On the basis of cracking pattern information, it can be concluded that CH_4 is released from the surface during precursor dosing. Similar to thermal ALD, the detection of CH_4 indicates that the $Al(CH_3)_3$ precursor chemisorbs to the surface through a reaction, in which H is removed from the surface by forming gaseous CH_4 with a $-CH_3$ ligand of the $Al(CH_3)_3$. During the plasma exposure peaks appear at $m/z=18$ (H_2O^+), 44 (CO_2^+), and 28 (CO^+), signaling the production of H_2O, CO_2, and possibly CO as discussed in our previous work.[22] Furthermore the consumption of oxygen during the plasma exposure can be clearly observed by the decrease of signal at $m/z=16$ and 32.

The CO^+ signal has a comparable intensity during the plasma exposure as the CO_2^+ signal. On the basis of the CO_2 cracking pattern reported in literature ($m/z=44$: 100% normalized peak height, $m/z=28$: 10%) it is therefore conceivable that CO is present in the deposition chamber.[54] The deviation from the literature values for CO_2 can, however, also be attributed to a lower transmission of high masses in the mass spectrometer. A dedicated experiment has, therefore, been performed to investigate the ratio of CO and CO_2 in the plasma by calibrating our mass spectrometer signals. CO_2 and CO gas from lecture bottles was introduced separately into the deposition reactor and a cracking spectrum of both species was determined at a pressure of 7.5 mTorr. The cracking of CO_2 was found to lead to the detection of mainly CO_2^+ ($m/z=44$: 100%), CO^+ ($m/z=28$: 18%), O^+ ($m/z=16$: 25%), and C^+ ($m/z=12$: 20%). The cracking of CO led to the detection of mainly CO^+ (100%) and some O^+ (4%) and C^+ (7%). To determine the gas composition at the start of the plasma exposure during processing, an experiment was carried out in which O_2 gas was mixed with CO and CO_2 in the reactor keeping the total pressure constant at 7.5 mTorr. From tuning the ratio of O_2, CO, and CO_2 to the peak height of the signals measured during processing, an estimate of the gas composition could be determined. On the basis of these measurements it was found that the concentrations of CO and CO_2 in the plasma are comparable in magnitude and that they form a substantial part of the total gas composition at the start of the plasma exposure ($\sim$7 and $\sim$5 vol % for CO and CO_2, respectively).

These results indicate that during the O_2 plasma exposure the surface bonded $-CH_3$ ligands are removed by combustionlike reactions, while the Al atoms at the surface are oxidized to form an Al_2O_3 film.[22] In the combustionlike reactions H_2O and CO_2 are produced, whereas the origin of CO could either be through incomplete combustion of the surface ligands or through dissociation of CO_2 in the plasma. On the basis of the current mass spectrometry measurements these production mechanisms of CO cannot be uniquely distinguished from each other.

During the plasma exposure a signal rise can also be observed at $m/z=15$ (this is most clear during the second cycle shown in Fig. 6, where the $m/z=28$ and $m/z=44$ sig-

nals have been omitted for clarity). The $m/z=15$ peak is smaller in height and appears to be about twice as short in time when compared to the CO, CO_2, and H_2O peaks. The observation of a signal at $m/z=15$ indicates the formation of CH_4 during the plasma step. A direct observation of CH_4 through the detection of CH_4^+ at $m/z=16$ is obscured by a decrease in O^+ signal (also at $m/z=16$) due to the consumption of O_2. It is conceivable that CH_4 is produced in a concurrent thermal ALD-like reaction pathway in which H_2O, available from the combustionlike reactions, is consumed in reactions with neighboring -CH_3 groups to form –OH groups at the surface.[24,36] The fact that this peak is observed for shorter time than the other peaks could be related to the limited availability of –CH_3 at the surface due to the competition with the combustionlike reactions.

The gas phase species were also monitored by QMS for ALD cycles which included the use of 15 successive $Al(CH_3)_3$ exposures. In Fig. 7 the QMS signals for the mass-to-charge ratios of $m/z=15$ (CH_3^+) and $m/z=27$ (Al^+) are shown. The ratio $m/z=27$ can be attributed to the cracking of $Al(CH_3)_3$ in the mass spectrometer, whereas $m/z=15$ can be attributed to cracking of both $Al(CH_3)_3$ and CH_4.[55] Simultaneously, QCM measurements were carried out to monitor film growth as shown in Fig. 7(c). In this part of the figure the precursor dosing and plasma exposure have also been indicated. Unfortunately, already during the recovery of the QCM signal from the plasma induced artifact, the $Al(CH_3)_3$ dosing was started, which partly obscured the mass uptake. Still the $Al(CH_3)_3$ exposure can be observed as a sharp increase in mass uptake in Fig. 7(c). The recovery of the signal from the plasma interference continues during the subsequent exposures of the precursor. It is evident that the mass uptake by QCM is accompanied by a sharp peak in the CH_3^+ signal which is considerably higher for the first few $Al(CH_3)_3$ exposures [see Fig. 7(a)]. Since no signal for Al^+ is observed during these first few exposures, we can attribute the first few peaks in CH_3^+ signal to the cracking of CH_4 generated by the chemisorption of $Al(CH_3)_3$ on the surface, as reported above. The peak intensities of the CH_3^+ signal gradually decreases with the number of $Al(CH_3)_3$ exposures since less and less precursor chemisorps with each succeeding $Al(CH_3)_3$ exposure. After five to six $Al(CH_3)_3$ exposures the CH_3^+ peaks reach approximately a constant intensity at each additional exposure, whereas also a signal for Al^+ is now observed in the QMS data [see Fig. 7(b)]. For the remainder of $Al(CH_3)_3$ exposures, the Al^+ and CH_3^+ signal intensities have roughly the same peak height and both signals correlate to the dissociation of unreacted $Al(CH_3)_3$ in the QMS. Also after five to six $Al(CH_3)_3$ exposures no more mass uptake is observed with the QCM [see Fig. 7(c)], indicating that the surface reactions have reached saturation. These observations agree well with the growth rate saturation curves obtained by SE and QCM shown in Fig. 3. Since QMS is a volume based technique, the aforementioned observations indicate that all surfaces, i.e., not only the surface of the QCM crystal or the substrate, but also the reactor walls, are saturatively covered with $Al(CH_3)_3$ precursor after five to six successive $Al(CH_3)_3$ exposures. The measurements in Fig. 7 also indicate that the $Al(CH_3)_3$ introduced

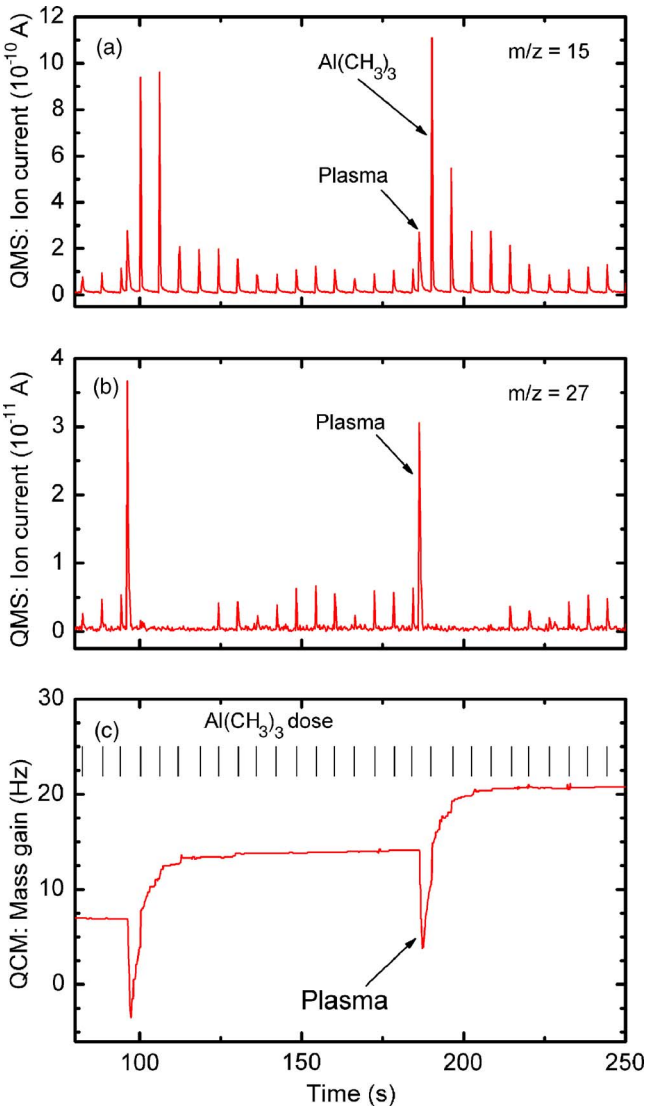

FIG. 7. (Color online) (a) QMS signal at $m/z=15$ and (b) at $m/z=27$ during an experiment in which 15 successive $Al(CH_3)_3$ exposures per cycle were applied. During the $Al(CH_3)_3$ exposures, the signal at $m/z=27$ can be attributed to $Al(CH_3)_3$ and the signal at $m/z=15$ to both CH_4 and $Al(CH_3)_3$. During plasma exposure the signal at $m/z=27$ can most probably be attributed to $C_2H_3^+$ created by dissociative ionization from higher hydrocarbon species. (c) Corresponding mass gain as measured by QCM. The $Al(CH_3)_3$ exposures are indicated by vertical tic marks in (c).

into the reactor is fully consumed by the surface reactions for the first five to six $Al(CH_3)_3$ exposures. Only when the surface reactions have saturated a significant density of $Al(CH_3)_3$ can build up in the gas phase leading to a QMS signal.

Another detail about the reaction mechanism is revealed by the QMS signal at $m/z=27$ during the plasma exposure in Fig. 7(a). A relatively high peak can be observed at $m/z=27$ during the plasma step and the signal intensity is more than a factor of 5 larger than that during $Al(CH_3)_3$ dosing. From a careful investigation of the other signals in the $m/z=24-28$ range we came to the conclusion that larger hydrocarbons (C_2H_x) are also present in the gas phase during the plasma exposure. This was not evident from our previous experiments,[22] as the signal at $m/z=28$ consists of contributions of CO^+ as well as $C_2H_4^+$. The absolute signals (ion

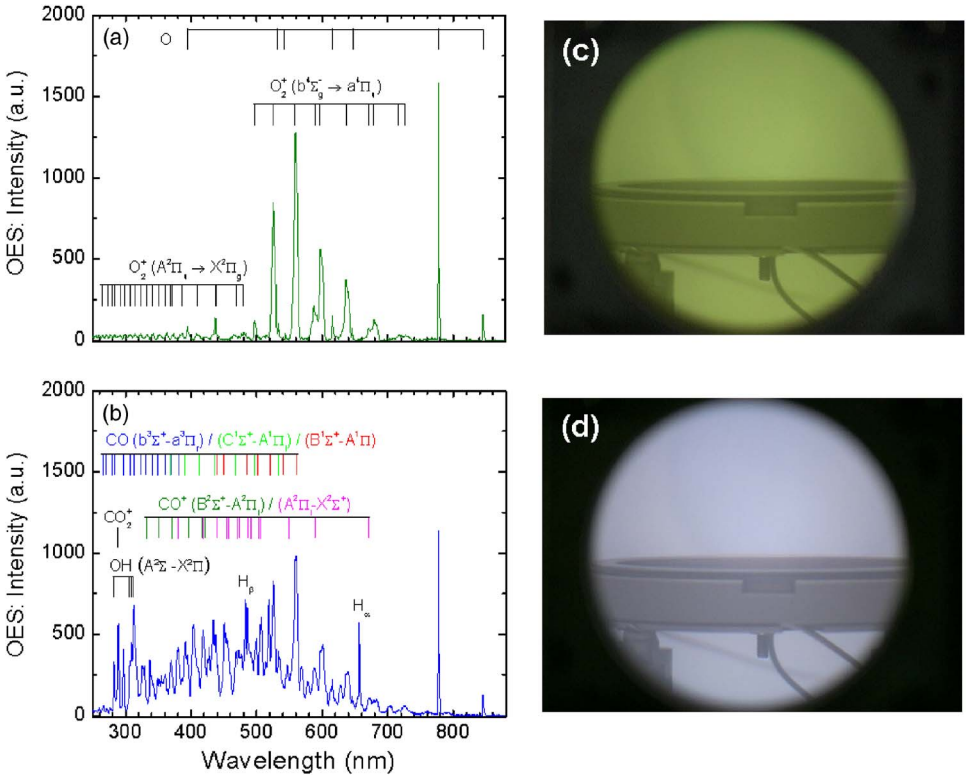

FIG. 8. (Color online) (a) OES from a pure O_2 plasma and (b) from the plasma after a preceding $Al(CH_3)_3$ dose recorded in the first 200 ms after the plasma strike. The different emission lines have been identified in the figure. (c) and (d) show photographs of the plasma corresponding to (a) and (b), respectively. The photographs are taken through the viewport at the side of the reactor and show the downstream region where the substrate holder is located.

current $\sim 3\times10^{-11}$ A) at $m/z=26$ and 27 are, however, a factor of 10 smaller compared to the CO^+ and CH_4^+ signals. On the basis of cracking pattern and cross-section data[56,57] it can be inferred that the production of these higher hydrocarbons is only a minor effect. It indicates, however, an alternative, third pathway in plasma-assisted ALD next to the already discussed combustionlike and thermal ALD-like reactions.

D. Monitoring excited plasma species and reaction products by OES

Specific to plasma-assisted ALD is the emission of light by plasma species during the plasma exposure step. This light emission provides an additional tool in the study of the gas composition and chemistry as the emission lines observed originate from radiative de-excitation of the gas species present in the plasma. These gas species can be both reactant or reaction products, and consequently these species can be identified by the use of optical emission spectroscopy.[22,37] In Fig. 8(a) the emission spectrum of a pure O_2 plasma is shown as collected in the proximity of the position of the substrate holder. The use of a quartz window provided better sensitivity in the UV region <350 nm compared to our earlier results in which a glass window was applied.[22] The identification of the various emission lines is given in Fig. 8(a). In the spectra mainly emission lines of excited O radicals (denoted as O*) and of O_2^+ ions from the first $(b\ ^4\Sigma_g^- - a\ ^4\Pi_u)$ and second $(A\ ^2\Pi_u - X\ ^2\Pi_u)$ negative systems are visible. This emission gives rise to the greenish color of the plasma which can also be observed around the substrate holder as shown in the photograph in Fig. 8(c). The photograph is taken from a window fitted at the side of the deposition chamber.

When an $Al(CH_3)_3$ dose has preceded the plasma exposure, the emission in the first hundreds of milliseconds of the plasma exposure is remarkably different from that of the pure O_2 plasma.[22] In the spectrum, taken at 200 ms after the start of the plasma exposure, an intense broadband emission in the blue region can be observed [Fig. 8(b)]. The plasma appears bluish to the naked eye, as is also apparent from the photograph in Fig. 8(d). From identification of the spectral lines, the broadband emission was found to be predominantly originating from excited CO* molecules. The bands from the Angström $(B\ ^1\Sigma^+ - A\ ^1\Pi_i)$, Herzberg $(C\ ^1\Sigma^+ - A\ ^1\Pi_i)$, and third positive $(b\ ^3\Sigma^+ - a\ ^3\Pi_r)$ systems of CO* as well as the Comet tail $(A\ ^2\Pi_i - X\ ^2\Sigma^+)$ and Baldet-Johnson $(B\ ^2\Sigma^+ - A\ ^2\Pi_i)$ systems of the CO^{+*} ion were identified as indicated in Fig. 8(b). Also the emission by atomic hydrogen (H_α and H_β) and atomic oxygen (777 and 845 nm) can be observed. In the UV region, OH* emission $(A\ ^2\Sigma^+ - X\ ^2\Pi)$ can be clearly distinguished from its typical band head structure around 309 nm as well as CO_2^{+*} from the double band structure $(\Gamma\ ^2\Sigma^+ - X\ ^2\Pi)$ present at 288.4 and 289.5 nm. Other lines in this UV region can most probably be assigned to CO*, in particular, to its third positive $(b\ ^3\Sigma^+ - a\ ^3\Pi_r)$ system, however, also the observation of lines from Al* and Al^{+*} [e.g., Al at 309.3 nm $(3s^2 3d - 3s^2 3p)$ and Al^+ at 281.6 nm $(3s4s - 3s3p)$, 286.8 nm $(3s9p - 3s3d)$, and 308.9 nm $(3s6d - 3s4p)$] cannot be excluded. Furthermore, the O_2^{+*} ion emission and O* radical emission are reduced in intensity at this early time after the start of the plasma exposure in the ALD cycle when compared to the emission during the continuous plasma operation [Fig. 8(a)].

The CO*, OH*, and H* emission most probably originates from excitation reactions of the molecules by electron impact. The excitation can either result from dissociative ex-

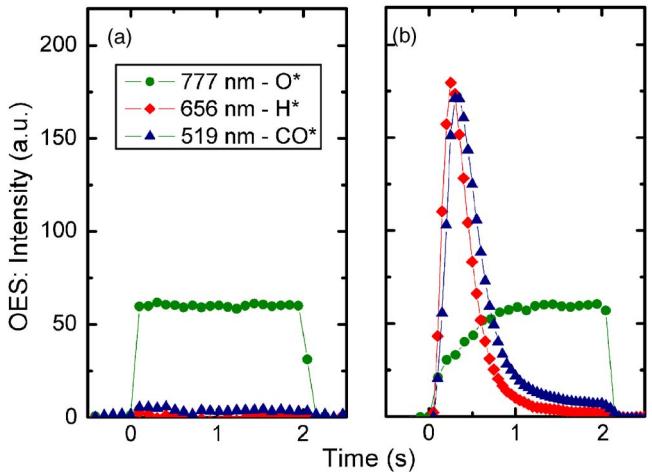

FIG. 9. (Color online) Time-resolved OES measurements at the wavelengths of 519, 656, and 777 nm corresponding to CO*, H*, and O*, respectively. (a) Emission for an O_2 plasma without preceding $Al(CH_3)_3$ dosing and (b) the emission for a plasma exposure step during an ALD cycle.

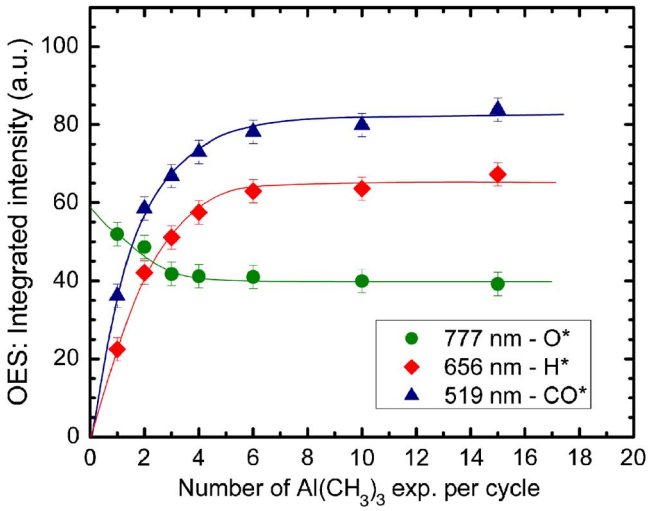

FIG. 10. (Color online) Integrated intensity of the time-resolved OES measurements of CO*, H*, and O* during the plasma step of the ALD cycle as a function of the number of successive $Al(CH_3)_3$ exposures used in the cycle.

citation or ionization of H_2O and CO_2 reaction products or from direct excitation and ionization of CO and H:[58]

$$H_2O + e^- \rightarrow OH^* + H + e^- \rightarrow OH + H^* + e^-, \quad (6)$$

$$H + e^- \rightarrow H^* + e^-,$$

$$CO_2 + e^- \rightarrow CO^* + O + e^- \rightarrow CO^{+*} + O + 2e^-, \quad (7)$$

$$CO + e^- \rightarrow CO^* + e \rightarrow CO^{+*} + 2e^-. \quad (8)$$

The threshold for these reactions is in the range of 10–25 eV, which are energies not uncommon in the inductively coupled plasma for electrons within the high energy tail of the electron energy distribution.[37,58] The possible presence of Al emission lines could potentially be related to a small fraction of (physisorbed) $Al(CH_3)_3$ residing in the reactor after precursor dosing (see Sec. IV A). When the surface reactions are completed and the reaction products are being pumped away, the reaction product related emission decreases. When approaching the end of the plasma exposure the emission is again identical to that of a pure O_2 plasma.

Observed by the naked eye, it appears that a kind of blue "flash," i.e. blue to green transition, occurs during the plasma exposure of each ALD cycle.[59] In Fig. 9 the time-resolved emission at 519 nm (CO*, Angström system v-$v'=0-2$), at 656 nm (H^*, H_α), and 777 nm (O*, $3p\ ^5P-3s^5S$) is shown for both a pure O_2 plasma strike and one which was preceded by an $Al(CH_3)_3$ dose (i.e., during an ALD cycle). During a pure O_2 plasma exposure [Fig. 9(a)] it can be observed that a stable O* emission is present at 777 nm instantly when the plasma was ignited. No significant emission signal is observed at 519 and 656 nm. When the plasma was ignited during the ALD cycle, a clear increase in emission at 519 and 656 nm can be observed at the beginning of the plasma exposure due to the build up of reaction products CO, (CO_2, and H_2O) in the gas phase [see Fig. 9(b)]. This increase is followed by a decrease in emission of the reactants due to the removal of the species by pumping when the surface reactions reach saturation. In the beginning of the plasma pulse the consumption of O radicals is also apparent from the initially lower emission intensity at 777 nm. This O* emission is lower as oxygen is used to generate CO, CO_2 and H_2O reaction products as well as to oxidize the Al on the surface. Subsequently, the O* intensity increases and at the end of the plasma exposure it levels off at the same height as in a pure O_2 plasma.

Besides giving insight into the reaction mechanisms, the time dependent OES signals in Fig. 9 also yield insight into the plasma exposure time necessary for reaching saturation. From the time-resolved signal of the CO* and H* emission, for which a $1/e$ decay time of ~300 ms can be determined, it can be concluded that the surface reactions and removal of reactants during the plasma step occur in a time span well within 1 s. This was corroborated by *in situ* spectroscopic ellipsometry measurements of films deposited under different plasma conditions. These measurements revealed a saturation of the growth rate for plasma exposure times >0.5 s.

Optical emission spectroscopy, which is a volume based technique similar to QMS, probes the saturation of the surface reactions on all the different surfaces of the reactor. To learn about the saturation behavior of the $Al(CH_3)_3$ precursor reactions, time dependent measurements of the reaction products were performed for different $Al(CH_3)_3$ doses. The time-resolved signals of O*, H*, and CO* were integrated and plotted as a function of the preceding precursor dose, expressed in the total number of successive $Al(CH_3)_3$ exposures per cycle, in Fig. 10. Clearly the saturation of surface reactions can be observed on the basis of the amount of H* and CO* emission during the plasma exposure. The integrated signals saturate at a dose of approximately six successive $Al(CH_3)_3$ exposures per cycle as also found with SE, QCM, and QMS, discussed earlier. Furthermore, the amount

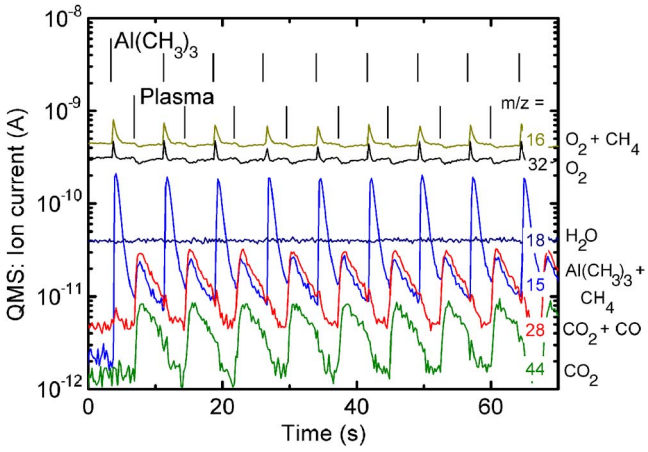

FIG. 11. (Color online) Time-resolved QMS during several plasma-assisted ALD cycles of Al_2O_3 carried out in the Oxford Instruments FlexAL reactor. The most likely parent molecules contributing to the signals at the selected mass-to-charge ratios (m/z) are given. The $Al(CH_3)_3$ dosing and plasma exposures are indicated in the figure.

of oxygen consumed can also be observed to increase in the nonsaturated region by a decrease in the integrated O* emission with increasing $Al(CH_3)_3$ dose.

E. QMS and OES results on the FlexAL reactor

To test the general validity of the results obtained on the ALD-I reactor, QMS and OES studies were also performed during the deposition of Al_2O_3 in the FlexAL reactor. The experiments were carried out without heating the reactor walls and substrate holder, i.e., at 25 °C. At this temperature a considerable fraction of the $Al(CH_3)_3$ might be in the dimer phase.[39,41] However, to the best of our knowledge, there have been no reports that this dimer phase has a substantial influence on the surface chemistry during ALD at low temperatures.

Measurements by QMS, which had a better signal-to-noise ratio at higher m/z ratios for the FlexAL than for the ALD-I reactor, revealed signals at $m/z=57$ $[Al(CH_3)_2^+]$, $m/z=42$ $[Al(CH_3)^+]$, $m/z=27$ (Al^+), and $m/z=15$ (CH_3^+) for the unreacted precursor. The peak heights were found to correspond well to the $Al(CH_3)_3$ cracking pattern reported under room temperature conditions.[55]

In Fig. 11 the time dependent signals of selected masses are given for a number of ALD cycles covering the same span as in Fig. 6. The moment of precursor dosing (20 ms duration) and period of plasma exposure (4 s duration) have been indicated. The chemisorption of $Al(CH_3)_3$ can be observed through the detection of CH_4, both on $m/z=15$ (CH_3^+) and $m/z=16$ (CH_4^+) as shown in Fig. 11. During precursor injection the signal rises also slightly for $m/z=32$. This increase is smaller than for $m/z=16$ and we attribute the increase at $m/z=32$ to the pressure increase in the QMS induced by the precursor injection. Albeit less clear, during the plasma exposure a decrease in the signals at $m/z=16$ and 32 can also be observed similar to the case in the ALD-I reactor as discussed above. This decrease can be explained by the consumption of oxygen by the oxidation of the surface and the production of combustionlike reaction products. These reaction products created during the plasma step are observed at $m/z=28$ (CO^+) and $m/z=44$ (CO_2^+). From the relative intensity of the CO^+ and CO_2^+ signals, it can be concluded that both CO_2 and CO are present in the plasma similar to the case in the ALD-I reactor. The production of H_2O during the plasma exposure cannot be distinguished at $m/z=18$. The absence of a clear signal rise at $m/z=18$ can be attributed to the relatively high pressure and therefore high background signal in the QMS on the FlexAL reactor in comparison with the QMS on the ALD-I reactor. The background signal at $m/z=18$ is approximately a factor of 10 higher in Fig. 11 than in Fig. 6, while the signal at $m/z=32$ due to the O_2 injected is quite comparable for the FlexAL and ALD-I. The signal at $m/z=32$ is only slightly higher in the FlexAL due to the higher operating pressure in the reactor (15 mTorr instead of 7.5 mTorr). The higher background pressure due to residual gases in the QMS and the corresponding higher baseline signal for $m/z=18$ (H_2O^+ due to residual H_2O) prevent therefore the detection of the relatively small H_2O levels generated during the plasma exposure step. A factor contributing to the higher H_2O pressure and background H_2O signal could be the lower wall temperature used in the experiments on the FlexAL reactor compared to the ALD-I reactor. This lower wall temperature will complicate efficient pumping of H_2O produced in the combustionlike reactions given the short cycle time of 7.5 s. This will lead to a built up to a relatively high H_2O background pressure in the reactor and mass spectrometer. Although a clear H_2O signal rise is absent during the plasma exposure, an increase at $m/z=15$ is still clearly observed providing evidence that the concurrent thermal ALD-like reactions are taking place in addition to the combustionlike reactions. This is an indirect indication of H_2O production during the plasma exposure step. Furthermore, similar as in the experiments on the ALD-I reactor a mass scan of $m/z=20-30$ in the FlexAL revealed the presence of small amounts of larger hydrocarbons (C_2H_x) during the plasma exposure as shown in Fig. 12. Compared to the CH_4^+ and CO^+ signals during the plasma exposure step, the signals due to the higher hydrocarbons were approximately ten times lower in magnitude (ion current of $\sim 3\times 10^{-12}$ A). Similar to the case of the ALD-I setup (see Sec. III C), it can be inferred from this data that the production of these higher hydrocarbons is a minor effect.

In comparison to the QMS results obtained on the ALD-I setup, the signals at the various m/z ratios decay with longer time constants for the FlexAL reactor. For a part, these longer time constants can be attributed to a longer residence time in the FlexAL reactor. When the decay of the $m/z=16$ signal during $Al(CH_3)_3$ exposure is fitted with a single exponential value, $\tau=\sim 0.17$ s and $\tau=\sim 0.45$ s are found for the ALD-I and FlexAL reactor, respectively. Both values are close to the mean residence time t_R in the ALD-I ($t_R=\sim 0.2$ s) and FlexAL ($t_R=\sim 0.4$ s). However, during the plasma exposure there appears to be another effect. The characteristic decay times of CO and CO_2 appear to be much longer ($\tau\sim 6$ s) in the FlexAL reactor than what would generally be expected on the basis of the residence time of $t_R=\sim 0.4$ s. For the ALD-I reactor this is not observed and the

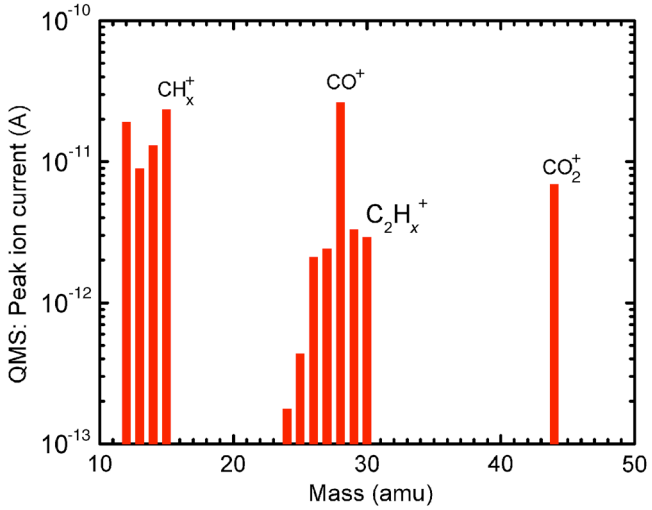

FIG. 12. (Color online) Bar graph mass spectrum during the O_2 plasma step as composed from the time-resolved quadrupole mass spectrometry (QMS) measurements carried out in the Oxford Instruments FlexAL reactor. The spectrum has been corrected for (background) signals during regular O_2 plasma operation and shows therefore only species that are related to the ALD surface reactions taking place during the O_2 plasma step. The most likely ions contributing to the signals at the selected mass-to-charge ratios (m/z) are indicated.

characteristic decay times of CO and CO_2 are similar to the residence time ($t_R = \sim 0.2$ s). This discrepancy is not yet understood.

As described in Sec. II B, the OES measurements on the FlexAL were performed through a quartz window at the top of the plasma source. In Fig. 13(a) a spectrum of a pure O_2 plasma is shown with the various O* and O_2^{+*} lines identified. Recall that both the emissions from the plasma source region and from the downstream reactor region are probed line of sight in the OES configuration on the FlexAL. The 400 W plasma generates a large amount of O* radical emission at 777 nm which saturated the detector, as indicated. Figure 13(b) shows the emission observed during the plasma exposure step of an ALD cycle. The emission is collected at the beginning of the plasma exposure ($t = \sim 200$ ms after plasma ignition). It is evident that a large amount of O_2 plasma-related emission is still present, probably most prominently generated in the plasma source itself. The presence of H_2O in the plasma can be deduced from the strong H* emission at 656 nm (H_α) and OH* emission around 309 nm ($A\ ^2\Sigma^+ - X\ ^2\Pi$ band head). This provides additional evidence that H_2O is produced in the FlexAL reactor despite the fact that the H_2O signal was obscured in the QMS data. Furthermore, compared to the pure O_2 plasma [Fig. 13(a)], the spectrum during the ALD processing [Fig. 13(b)] also shows a clear broadband emission. Although no clearly resolved CO* related peaks can be distinguished, the subtraction of both spectra in Fig. 13 confirms the presence of CO* emission.

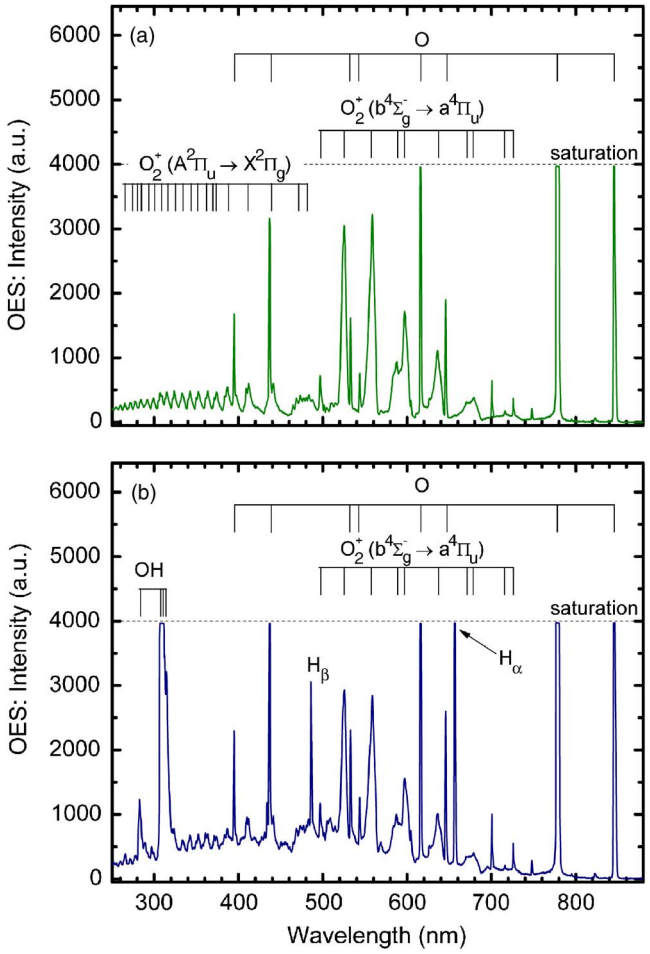

FIG. 13. (Color online) (a) OES from a pure O_2 plasma and (b) from the O_2 plasma after a preceding $Al(CH_3)_3$ dose recorded in the first 200 ms after the plasma strike. The spectra were taken through the top viewport on the plasma source of the Oxford Instruments FlexAL reactor. The different peaks have been identified in the spectra and the saturation level of the spectrometer is indicated.

IV. DISCUSSION

A. Reaction mechanism for plasma-assisted ALD of Al_2O_3

In the previous section, the plasma-assisted ALD process of Al_2O_3 from $Al(CH_3)_3$ and O_2 plasma has been investigated in two remote plasma ALD reactors by four different *in situ* diagnostics. With respect to the reaction mechanism of Al_2O_3, the results can be summarized in the following major observations:

(i) In the precursor dosing step, the chemisorption of $Al(CH_3)_3$ takes place by the release of CH_4 in the gas phase.

(ii) At a substrate temperature of 70 °C, $Al(CH_3)_3$ predominantly chemisorbs bifunctionally to the surface, i.e., it reacts predominantly with two surface groups.

(iii) Because the process window of plasma-assisted ALD extends down to room temperature, all internal surfaces of the reactor (i.e., also the reactor walls) contribute to $Al(CH_3)_3$ consumption during the precursor dosing step. A significant gas phase density of $Al(CH_3)_3$ build up only in the reactor when the reactions at all the internal surfaces reach saturation.

(iv) During the O_2 plasma exposure, the oxygen in the plasma is significantly consumed by the oxidation of the Al_2O_3 surface and the combustion of $-CH_3$ surface groups.

(v) The combustion of the $-CH_3$ surface groups leads to

the production of CO, CO_2, and H_2O reaction products. The presence of CO in the plasma can indicate incomplete combustion reactions but can also be cause by the dissociation of CO_2 in the plasma.

(vi) CH_4 is also a reaction product during the O_2 plasma exposure step. From the height of the CH_4 signal and its time response, it is concluded that the CH_4 is created in a concurrent thermal ALD-like reaction pathway initiated by the H_2O produced in the combustionlike reactions of the $–CH_3$ groups. This secondary reaction competes with the combustionlike reactions. It is, however, a minor effect as it requires first the production of H_2O, while it can only be significant during the time when there are still $–CH_3$ groups present at the surface.

(vii) The presence of higher hydrocarbons (C_2H_x) is also observed during the O_2 plasma exposure step indicating a possible third reaction pathway.

(vii) At the beginning of the plasma exposure step, large quantities of reaction products are released into the plasma because $Al(CH_3)_3$ has been chemisorbed at all internal surfaces of the reactor. This leads to significant disturbance of the O_2 plasma properties as the reaction products undergo ionization and dissociation reactions in the plasma.

On the basis of these observations the following qualitative picture of the reaction mechanism during plasma-assisted ALD of Al_2O_3 can be deduced. The surface reactions during $Al(CH_3)_3$ dosing in plasma-assisted ALD appear to be very similar to those in thermal ALD. In both cases CH_4 is released as a reaction product during the chemisorption of $Al(CH_3)_3$ on the surface. For both plasma-assisted ALD and thermal ALD it appears that $Al(CH_3)_3$ chemisorbs mostly bifunctionally on the surface, at least at the low substrate temperatures investigated.[24] Information on the surface groups involved during $Al(CH_3)_3$ chemisorption cannot be directly deduced from the data. However, from the fact that CH_4 is released from the surface, it can be concluded that H atoms are available on the surface for the reaction with the $–CH_3$ ligands of the chemisorbing $Al(CH_3)_3$.

The oxidation step during plasma-assisted ALD is very different from the oxidation step during thermal ALD with H_2O. Oxygen radicals are the dominant species in an (inductively coupled) O_2 plasma[60] and therefore rule the surface reactions during the oxidation step. These O radicals are consumed in the oxidation of the Al atoms on the surface and the combustion of the $–CH_3$ surface groups. This consumption of O radicals leads to a change in the mass balance in the plasma, decreasing the O and O_2 density levels during the time interval that the surface reactions take place. The reaction of the O radicals with the $–CH_3$ surface groups leads to several reaction products. Most important is the combustion of the $–CH_3$ surface groups leading to CO, CO_2, and H_2O reaction products in the gas phase. The fact that CO is observed in the plasma can indicate incomplete combustion reaction, however, from the data reported CO production from incomplete combustion cannot be distinguished unambiguously from the production of CO in the gas phase by dissociation of CO_2 molecules in the plasma. This latter reaction will certainly also take place. A second reaction pathway during the O_2 plasma step is initiated by the H_2O produced by the combustionlike reactions. Once H_2O is produced from a $–CH_3$ surface group it can react with a neighboring $–CH_3$ surface group by a thermal ALD-like reaction. This secondary reaction competes therefore with the combustionlike reactions but it can only take place during the time when there are still $–CH_3$ groups present at the surface. This reaction pathway becomes insignificant at the moment when almost all $–CH_3$ surface groups are reacted away by the combustionlike reactions. A third reaction pathway is indicated by the observation of higher hydrocarbon species (C_2H_x) in the plasma. The observation of such higher hydrocarbons suggests that the oxygen radicals are not effective in combusting all $–CH_3$ surface groups. Consequently, it makes it more plausible that the combustionlike surface reactions are incomplete and that CO is also directly produced at the surface. The production of higher hydrocarbon species appears to be a minor effect, however, some of the higher hydrocarbon species can also be oxidized by combustionlike reactions with oxygen species in the gas phase.[61] The higher hydrocarbon species can be generated at the surface by reaction mechanisms as proposed by Elliott *et al.*[20] When O radicals attack the bonds within the $–Al–CH_3$ surface groups, intermediate surface groups can be formed such as $–Al–O–CH_3$ (methoxy groups) or $–Al–CH_2OH$. Subsequently, volatile higher hydrocarbon species (C_2H_x) can be formed. For example, by association reactions between neighboring $–CH_2$ surface groups, ethene (C_2H_4) can be formed. On the basis of first principles density functional theory calculations it has been found that such reaction pathways might be energetically favored over combustionlike reactions.[20] It should, however, be noted that the preference for certain surface reaction pathways is also determined by the flux of the incoming O radicals. During the O_2 plasma exposure there is a relatively high flux of O radicals to the surface,[60] which can cause the combustionlike reactions to be favored.

Although the reaction mechanism presented can explain most observations and is expected to describe the main surface reactions, other and additional reaction mechanisms can not be excluded. For example, an alternative explanation for the formation of higher hydrocarbons can be sought in the presence of physisorbed $Al(CH_3)_3$ at the surface during the precursor exposure. While it should be noted that $Al(CH_3)_3$ will predominantly chemisorb, a small fraction of physisorbed $Al(CH_3)_3$ can possibly be present, in particular, at high precursor doses and low substrate temperatures as under these conditions, adsorbed $Al_2(CH_3)_6$ multilayers have been reported (albeit at much higher gas pressures).[62] During the plasma exposure the physisorbed molecules will be released into the gas phase and subsequently be dissociated by the plasma. The fragmented hydrocarbon species can associate to form higher hydrocarbons and can explain the observation of C_2H_x species by mass spectrometry [see Figs. 7(b) and 12]. In addition, this effect can explain the possible presence of Al^* and Al^{+*} emission lines in the plasma although these lines cannot be unambiguously distinguished from the spec-

tra in Figs. 8(b) and 13(b) due to the interfering presence of OH^*, CO_2^{+*}, and CO^* lines in the UV region.

The large quantities of reaction products that are released into the plasma at the beginning of the plasma step have a substantial effect on the plasma properties. The reaction products become dissociated and ionized in the plasma, thus changing the composition of the plasma significantly. As a consequence the impedance of the plasma can also be altered, which might affect plasma power coupling and drift in the optimum power matching conditions. In addition the change in plasma composition can also lead to secondary effects at the surface, for example, redeposition reactions can occur. These effects, caused by the surface reaction products, increase in importance with increasing inner surface area of the reactor because under saturated conditions $Al(CH_3)_3$ has been chemisorbed at all internal surfaces of the reactor.

As mentioned earlier, information on the surface groups created after O_2 plasma exposure of the $-CH_3$ terminated surface cannot directly be deduced from the reaction product data. The fact that CH_4 is released from the surface during $Al(CH_3)_3$ dosing indicates, however, that H atoms are present at the surface after O_2 plasma exposure. This aspect, as well as the observation that the temperature dependence of the growth rate per cycle of plasma-assisted and thermal ALD show remarkable similarities[3] (most notably at higher substrate temperatures) might suggest the presence of hydroxyl (–OH) surface groups after the O_2 plasma step. Such –OH surface groups can possibly be created directly in the combustionlike reactions, but they can also be created indirectly by the H_2O molecules generated at the surface in the combustionlike reactions. The presence of –OH surface groups after the oxidation step has also been predicted for ALD of Al_2O_3 using O_3 as oxidant source[20] although experimental investigations showed some variance.[21] Possible differences between results obtained with O_3 as oxidant source and between the O_3 and O_2 plasma case can possibly be attributed to differences in the flux of reactive species to the surface during the oxidation step. A difference in flux and related surface chemistry can also possibly explain differences in growth rates per cycle observed for the different oxidant sources.[3] More insight into the surface reactions and the surface groups present after the O_2 plasma step will be provided by *in situ* infrared spectroscopy measurements of the surface groups. These infrared spectroscopy measurements are currently carried out and will be reported in a future publication.[63]

B. Consequences for other plasma-assisted ALD processes

The qualitative picture of the reaction mechanism for plasma-assisted ALD of Al_2O_3 described above can most probably be generalized to other plasma-assisted ALD processes of metal oxide films employing O_2 plasma as oxidant source. It is expected that the reaction mechanism is similar when using other metal alkyl compounds as precursor, whereas it is also anticipated that roughly the same reaction mechanism holds for oxide films deposited by ALD from metal organic precursors and O_2 plasmas in general. During the precursor dosing, the chemisorption reactions are expected to specifically depend on the precursor, most notably on the nature of its organic ligands. The O_2 plasma step is, however, expected to be ruled by combustionlike reactions due to the large O flux in an O_2 plasma. Also secondary reactions such as initiated by H_2O by-products are expected to play a role for other plasma-assisted ALD processes employing metal organic precursors. In addition, for other metal organic compounds (metal alkoxide, alkylamide, beta-diketonate, etc.) also other types of reaction products than CO_2, CO, H_2O, and hydrocarbon species might be formed during the O_2 plasma step depending on the atomic composition of the organic ligands. For example, for metal alkylamide precursors and O_2 plasma, the formation of CN and NO-related species can be anticipated. The level of influence of these and other reaction products on the plasma properties depends on the ALD process characteristics. For example, when the precursor does not chemisorb on the reactor walls for a cold-wall reactor, the influence of the reaction products released from the heated substrate holder during the O_2 plasma step will be relatively minor. Insight in these and other aspects of plasma-assisted ALD of metal oxides from metal organic precursors and O_2 plasma can be obtained relatively easy by mass spectrometry and optical emission spectroscopy studies as shown in this work.

V. CONCLUSIONS

The reaction mechanism of the plasma-assisted ALD process of Al_2O_3 from $Al(CH_3)_3$ dosing and O_2 plasma exposure was investigated. Results were combined from four complementary *in situ* diagnostics. With spectroscopic ellipsometry and quartz crystal microbalance measurements, the thickness increase and mass gain per cycle was monitored, whereas with quadrupole mass spectrometry and optical emission spectroscopy, the reaction products created during the ALD surface reactions were investigated. Aspects such as $Al(CH_3)_3$ chemisorption and its saturation behavior, combustionlike reactions and additional reaction pathways during O_2 plasma exposure leading to hydrocarbon species, and the influence of the reaction products on the O_2 plasma properties were discussed. From a comparison with thermal ALD of Al_2O_3 and the main observations made, a qualitative picture of the reaction mechanism of plasma-assisted ALD of Al_2O_3 was presented. To achieve a higher level of understanding of the reaction mechanism, experimental data on the surface functional groups created by the ALD half-reactions will be required. Such information can be obtained by infrared spectroscopy measurements that are currently carried out for plasma-assisted ALD of Al_2O_3.

It has also been discussed that the results on the reaction mechanism obtained for Al_2O_3 can most probably be generalized for plasma-assisted processes of metal oxides employing metal alkyl compounds and even for metal organic precursors in general. From the results presented in this work, it has become clear that considerable insight into the reaction mechanisms of plasma-assisted ALD processes of other metal oxides can be obtained by common diagnostics such as quadrupole mass spectrometry and optical emission spectros-

copy. Especially optical emission spectroscopy has turned out to be a relatively simple and inexpensive diagnostic which can easily be applied to (commercial) plasma-assisted ALD reactors while providing much more information than only the oxygen species present in the steady-state O_2 plasma employed. The *in situ* diagnostics will therefore also be employed in future studies of the plasma-assisted ALD processes of other metal oxide films deposited from different kinds of metal organic precursors.

ACKNOWLEDGMENTS

The authors acknowledge A.J.M. Mackus and P. Kudlacek for their assistance with the measurements and Dr. R. Engeln for the fruitful discussions. M.J.F. van de Sande, W. Keuning, and J.J.A. Zeebregts are thanked for their skilful technical assistance. The authors would like to thank the reviewer for pointing out the possible presence of Al emission lines and the related consequences. The Dutch Technology Foundation STW is acknowledged for their financial support. The research of W.K. was made possible by a fellowship from the Royal Netherlands Academy of Arts and Sciences (KNAW).

[1]R. L. Puurunen, J. Appl. Phys. **97**, 121301 (2005).
[2]S. C. Ha, E. Choi, S. H. Kim, and J. S. Roh, Thin Solid Films **476**, 252 (2005).
[3]J. L. van Hemmen, S. B. S. Heil, J. H. Klootwijk, F. Roozeboom, M. C. M. van de Sanden, and W. M. M. Kessels, J. Electrochem. Soc. **154**, G165 (2007).
[4]J. W. Lim and S. J. Yun, Electrochem. Solid-State Lett. **7**, F45 (2004).
[5]S. K. Kim, S. W. Lee, C. S. Hwang, Y. S. Min, J. Y. Won, and J. Jeong, J. Electrochem. Soc. **153**, F69 (2006).
[6]M. J. Cho, D. S. Jeong, J. Park, H. B. Park, S. W. Lee, T. J. Park, C. S. Hwang, G. H. Jang, and J. Jeong, Appl. Phys. Lett. **85**, 5953 (2004).
[7]X. Y. Liu, S. Ramanathan, A. Longdergan, A. Srivastava, E. Lee, T. E. Seidel, J. T. Barton, D. Pang, and R. G. Gordon, J. Electrochem. Soc. **152**, G213 (2005).
[8]J. B. Kim, D. R. Kwon, K. Chakrabarti, C. Lee, K. Y. Oh, and J. H. Lee, J. Appl. Phys. **92**, 6739 (2002).
[9]T. M. Mayer, J. W. Elam, S. M. George, P. G. Kotula, and R. S. Goeke, Appl. Phys. Lett. **82**, 2883 (2003).
[10]B. Hoex, S. B. S. Heil, E. Langereis, M. C. M. van de Sanden, and W. M. M. Kessels, Appl. Phys. Lett. **89**, 042112 (2006).
[11]E. Langereis, M. Creatore, S. B. S. Heil, M. C. M. van de Sanden, and W. M. M. Kessels, Appl. Phys. Lett. **89**, 081915 (2006).
[12]S. J. Yun, Y. W. Ko, and J. W. Lim, Appl. Phys. Lett. **85**, 4896 (2004).
[13]T. T. Van and J. P. Chang, Appl. Phys. Lett. **87**, 011907 (2005).
[14]P. F. Carcia, R. S. McLean, M. H. Reilly, M. D. Groner, and S. M. George, Appl. Phys. Lett. **89**, 031915 (2006).
[15]A. P. Ghosh, L. J. Gerenser, C. M. Jarman, and J. E. Fornalik, Appl. Phys. Lett. **86**, 223503 (2005).
[16]M. D. Groner, S. M. George, R. S. McLean, and P. F. Carcia, Appl. Phys. Lett. **88**, 051907 (2006).
[17]G. Agostinelli, A. Delabie, P. Vitanov, Z. Alexieva, H. F. W. Dekkers, S. De Wolf, and G. Beaucarne, Sol. Energy Mater. Sol. Cells **90**, 3438 (2006).
[18]C. Bernay, A. Ringuede, P. Colomban, D. Lincot, and M. Cassir, J. Phys. Chem. Solids **64**, 1761 (2003).
[19]C. N. Ginestra, R. Sreenivasan, A. Karthikeyan, S. Ramanathan, and P. C. McIntyre, Electrochem. Solid-State Lett. **10**, B161 (2007).
[20]S. D. Elliott, G. Scarel, C. Wiemer, M. Fanciulli, and G. Pavia, Chem. Mater. **18**, 3764 (2006).
[21]D. N. Goldstein and S. M. George, Proceedings of the 6th AVS Topical Conference on ALD, Seoul, Korea, 2006 (unpublished).
[22]S. B. S. Heil, P. Kudlacek, E. Langereis, R. Engeln, M. C. M. van de Sanden, and W. M. M. Kessels, Appl. Phys. Lett. **89**, 131505 (2006).
[23]M. Juppo, A. Rahtu, M. Ritala, and M. Leskelä, Langmuir **16**, 4034 (2000).
[24]A. Rahtu, T. Alaranta, and M. Ritala, Langmuir **17**, 6506 (2001).
[25]M. D. Groner, F. H. Fabreguette, J. W. Elam, and S. M. George, Chem. Mater. **16**, 639 (2004).
[26]S. D. Elliott and J. C. Greer, J. Mater. Chem. **14**, 3246 (2004).
[27]Y. Widjaja and C. B. Musgrave, Appl. Phys. Lett. **80**, 3304 (2002).
[28]C. Soto and W. T. Tysoe, J. Vac. Sci. Technol. A **9**, 2686 (1991).
[29]A. C. Dillon, A. W. Ott, J. D. Way, and S. M. George, Surf. Sci. **322**, 230 (1995).
[30]A. W. Ott, K. C. McCarley, J. W. Klaus, J. D. Way, and S. M. George, Appl. Surf. Sci. **107**, 128 (1996).
[31]A. W. Ott, J. W. Klaus, J. M. Johnson, and S. M. George, Thin Solid Films **292**, 135 (1997).
[32]For simplicity only the reaction is given in which $Al(CH_3)_3$ reacts with one surface –OH group (i.e., monofunctionally). As discussed in Ref. 24, there is evidence that a considerable fraction of $Al(CH_3)_3$ reacts with two surface –OH groups (i.e., bifunctionally).
[33]F. A. Cotton, C. A. Murillo, and M. Bochmann, *Advanced Inorganic Chemistry* (Interscience, New York, 1988).
[34]R. L. Puurunen, Appl. Surf. Sci. **245**, 6 (2005).
[35]R. L. Puurunen, J. Appl. Phys. **95**, 4777 (2004).
[36]R. L. Puurunen, Chem. Vap. Deposition **9**, 327 (2003).
[37]S. B. S. Heil, E. Langereis, F. Roozeboom, M. C. M. van de Sanden, and W. M. M. Kessels, J. Electrochem. Soc. **153**, G956 (2006).
[38]E. Langereis, H. C. M. Knoops, A. J. M. Mackus, F. Roozeboom, M. C. M. van de Sanden, and W. M. M. Kessels, J. Appl. Phys. **102**, 083517 (2007).
[39]A. W. Laubengayer and W. F. Gilliam, J. Am. Chem. Soc. **63**, 477 (1941).
[40]K. S. Pitzer and H. S. Gutowsky, J. Am. Chem. Soc. **68**, 2204 (1946).
[41]S. Kvisle and E. Rytter, Spectrochim. Acta, Part A **40**, 939 (1984).
[42]S. F. Szymanski, M. T. Seman, and C. A. Wolden, J. Vac. Sci. Technol. A **25**, 1493 (2007).
[43]S. F. Szymanski, M. T. Seman, and C. A. Wolden, Surf. Coat. Technol. **201**, 8991 (2007).
[44]M. N. Rocklein and S. M. George, Anal. Chem. **75**, 4975 (2003).
[45]A. Rahtu and M. Ritala, Appl. Phys. Lett. **80**, 521 (2002).
[46]Absolute calibration of the mass gain proved to be inaccurate because the effective surface area of the QCM was ill defined. This is due to the fact that also a part of the backside of the QCM crystal is covered with Al_2O_3 by ALD.
[47]S. B. S. Heil, J. L. van Hemmen, C. J. Hodson, N. Singh, J. H. Klootwijk, F. Roozeboom, M. C. M. van de Sanden, and W. M. M. Kessels, J. Vac. Sci. Technol. A **25**, 1357 (2007).
[48]S. B. S. Heil, E. Langereis, A. Kemmeren, F. Roozeboom, M. C. M. van de Sanden, and W. M. M. Kessels, J. Vac. Sci. Technol. A **23**, L5 (2005).
[49]J. Kim, K. Chakrabarti, J. Lee, K. Y. Oh, and C. Lee, Mater. Chem. Phys. **78**, 733 (2003).
[50]A. Niskanen, K. Arstila, M. Ritala, and M. Leskelä, J. Electrochem. Soc. **152**, F90 (2005).
[51]S. J. Yun, J. W. Lim, and J.-H. Lee, Electrochem. Solid-State Lett. **7**, C13 (2004).
[52]R. Matero, A. Rahtu, M. Ritala, M. Leskelä, and T. Sajavaara, Thin Solid Films **368**, 1 (2000).
[53]A. Rahtu and M. Ritala, J. Mater. Chem. **12**, 1484 (2002).
[54]NIST/EPA/NIH Mass Spectral Library, Data Version NIST05, Software Version 2.0d.
[55]C. Q. Jiao, C. A. DeJoseph, P. Haaland, and A. Garscadden, Int. J. Mass. Spectrom. **202**, 345 (2000).
[56]T. Shirai, T. Tabata, H. Tawara, and Y. Itikawa, At. Data Nucl. Data Tables **80**, 147 (2002).
[57]O. J. Orient and S. K. Srivastava, J. Phys. B **20**, 3923 (1987).
[58]M. A. Lieberman and A. J. Lichtenberg, *Principles of Plasma Discharges and Materials Processing* (Wiley, New York, 1994).
[59]See EPAPS Document No. E-APPLAB-89-331639 for a movie of the plasma emission during a plasma-assisted ALD cycle. This document can be reached through a direct link in the online article's HTML reference section or via the EPAPS homepage http://www.aip.org/pubservs/epaps.html.
[60]J. T. Gudmundsson, I. G. Kouznetsov, K. K. Patel, and M. A. Lieberman, J. Phys. D **34**, 1100 (2001).
[61]I. Moller, A. Serdyuchenko, and H. Soltwisch, J. Appl. Phys. **100**, 033302 (2006).
[62]D. J. Ehrlich and R. M. Osgood, Chem. Phys. Lett. **79**, 381 (1981).
[63]E. Langereis, J. Keijmel, M. C. M. van de Sanden, and W. M. M. Kessels (unpublished).